

NUMERICAL TEST RIG FOR TURBINE GAS METER

*Toralf Hoch*¹, *Ernst von Lavante*²

¹RMG Messtechnik GmbH, D-35510 Butzbach, Germany, toralf.hoch@rmg.com

²University Duisburg-Essen, D-47057 Duisburg, Germany, ernst3.vonlavante@uni-due.de

Abstract – Generally, the determination of the performance and quality of volumetric flow meters is being carried out using so called error curves. They are the result of experiments performed on test rigs for different design variations and operating conditions. In order to augment this development process for flow meter to reduce costs in terms of money and time, computational fluid dynamics (CFD) software has been applied as the so called “Numerical Test Rig”. This “Numerical Test Rig” includes a full three-dimensional flow simulation of a realistic meter configuration. Close attention was paid to correct reproduction of the meter features, requiring simulation of the complete geometry with flow straightener, rotor and the downstream domain, all within a 360° circumference. A new algorithm to determine the error curves was developed based on the detailed consideration of inflow and outflow velocities. Equally, the realistic computation of the bearing friction forces and moments was implemented. Simulations of several test cases produced resulting error curves that compared favourably with curves measured for real meters.

Keywords: turbine gas meter, numerical simulation, test rig

1. INTRODUCTION

From an economical point of view of the customer and the vendor, the volume of sales of the gas has to be measured as accurately as possible. With respect to this requirement, the expectations imposed on the measuring systems are very high. The turbine gas meter is thought to fulfil all these needs and is capable of measuring very accurately the volumetric flow rate in a wide range of meter applications.

To assess the turbine meter performance and accuracy, a meter-characteristic error curve is used. Such line shows the deviation of a test meter from a reference meter as a function of the flow rate. New meter designs are evaluated by comparison with existing meters based on the corresponding error curves. The determination of the error curves is expensive, especially for high pressure applications, and very time consuming. During the last years, commercial CFD program systems made available represent powerful tools for flow investigations, being able to solve very complex problems accurately enough in acceptable time to be of practical use. These features make

CFD interesting for industrial applications as there is a growing demand to save cost and time.

In the past, most of the investigations of turbine flow meters accomplished using analytical and experimental methods. The number of publications dealing with, for example, friction forces, equation of motion, profile deformations and similar detailed flow considerations is relatively large. On the other hand, due to the high complexity of the flow field in a typical turbine flow meter the number of publications describing CFD simulations is rather small. Among the first industrial investigations of turbine meters using CFD were [1] and [2]. In these publications, only one blade-to-blade domain of the rotor was simulated due to computer size limitations. Based on velocity- and pressure distributions on the blade, a novel method of the determination of the error deviation was introduced. The simulation of the three-dimensional fully unsteady flow fields in a channel with one flow straightener and one rotor blade-to-blade space was carried out in [3]. The goal of [4] was to investigate the sources of inaccuracies in the flow measurement at low volumetric flow rates. It was showed that the secondary vortices formed a stagnation point on the upper casing that, in turn, caused in the laminar case a flow separation. A detailed analysis of the three-dimensional unsteady flow field in a turbine meter was given in [5] and [6]. Advices for the optimization of the meter design were given in [7]. In this work a numerical simulation of three-dimensional flow fields in a small turbine flow meter for liquids, including upstream and downstream flow conditioner, was performed. A method for predicting the meter features and performance and error curves was introduced as well.

The main goal of the present work was to develop a useful prediction tool for error curves during a design process of a new turbine flow meter. The present efforts included parameter variations in a given turbine flow meter for gases (DN80) as manufactured by the RMG along with the determination of the corresponding error curves. Initially, the CFD simulation was carried out for a reference meter for a constant meter factor K including 360° circumference in order to consider the effects of asymmetric inflow. The second step was to extract the velocities on planes close to the rotor inflow and outflow. These velocities were the main parameters for further investigations. Based on momentum change- and airfoil approaches in [8], the error curve including six operating points was obtained based on the moment coefficient c_m .

The resulting value included correction for bearing friction. The error curves were normalized by Q_{max} , making comparison of the relative curves for different design and operation cases plausible.

2. NUMERICAL SIMULATION

Pre-processing

Due to the complexity of the model and in order to save time, the turbine gas meter was designed using professional Computer Aided Design Software (CAD) and subsequently exported into a mesh generator. No design simplifications were implemented. The current grid generator, made the production of unstructured meshes for three domains (flow straightener, rotor and tailing domain) with 4.7 million nodes possible, considering the proper boundary layer resolution, see Fig. 1.

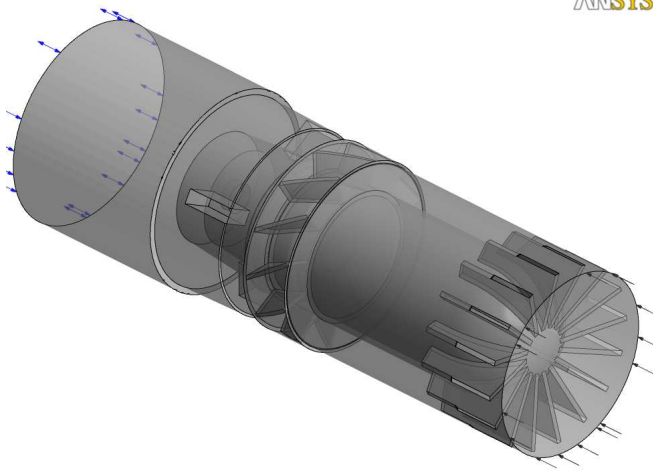


Fig. 1 Complete geometry used in the simulation (flow straightener, rotor and downstream domain)

Solver

In the present investigation, the commercial solver CFX was used, together the necessary definitions of the boundary conditions. These had to include the flow straightener inflow velocity, static pressure at the outflow and the rotor speed. The later analysis algorithm based on constant meter factor K made the formulation of the boundary conditions easier. The chosen turbulence model was the wall-distance free SST. Calculation time was approx. seven hours per operation point. The error curve was constructed from six points (5%, 10%, 25%, 40%, 70% and 100% of Q_{max})

Post-processing

For formation of the error curve, the velocities in the inflow and outflow planes in front and back of the rotor must be determined, see Fig. 2. The torque on rotor blades and rotor hub was equally important due to the presence of significant friction forces.

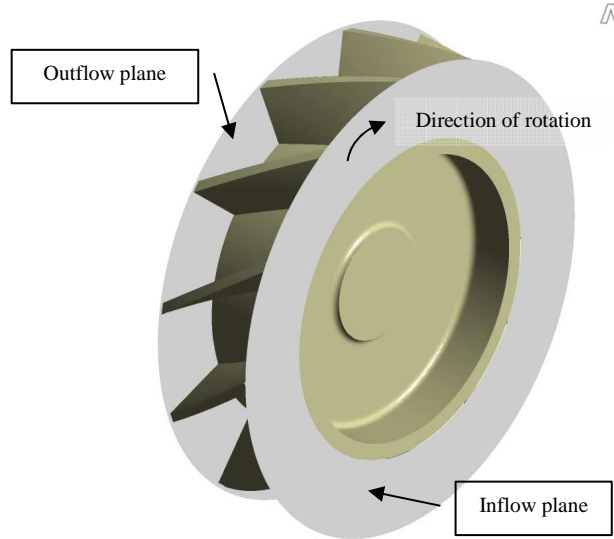


Fig. 2 Planes at inflow and outflow of the rotor

3. ANALYSIS ALGORITHM

The present investigation was based on the assumption of an ideal meter, meaning that the driving moments (momentum change and lift forces) and braking torques (form drag and friction forces) were in equilibrium. Turbine flow meters are a special version of turbines since the mechanical work has to be zero. An ideal meter would have a constant K -factor. In reality, however, mechanical work is needed to overcome the braking torque due to friction. The flow passes the cascade of the gas meter while being subjected to losses. The velocity decreases during the flow through the meter due to energy conversion in heat (dissipation). The analysis algorithm was based on an assumption that all the losses impose a reduction of the total pressure, thus causing a velocity reduction in the nearly incompressible flow. According to previous explanations the velocity difference can be used as a criterion for the meter evaluation. In engineering praxis, however, it is customary to use dimensionless parameters for comparisons of different configurations, leading to a somewhat different approach. The dimensionless relative moment coefficient c_m was employed as it includes the influence of the inflow and outflow velocity distributions.

A typical error curve diagram displays the volumetric flow deviation of test flow meter from a reference meter with a known relative measurement error. In this work, the relative error was substituted by the dimensionless moment coefficient c_m . For ideal conditions, the moment should be close to zero and the deviation is the difference from the real error curves. Reference (1) introduced a similar approach by computing the moment M from density ρ , inflow velocity u_{in} in the reference plane, projected area A and the cord length of the rotor blade L_{blade} .

$$M = c_m \cdot \frac{\rho}{2} \cdot u_{in}^2 \cdot A \cdot L_{blade} \quad (1)$$

The main assumption was that moments due to momentum change M_m or aerodynamic forces M_a complement each other and are thus averaged, resulting in equation (1a)

$$M = M_m + M_a = c_m \cdot \frac{\rho}{2} \cdot u_{in}^2 \cdot A \cdot L_{blade} \quad (1a)$$

Under the assumption that the total torque on the rotor is a superposition of drag and lift forces, the torque due to drag forces (viscosity forces due to friction, form drag forces) was computed using eq. (2), where r_{tip} and r_{hub} were the radii of the blade root and blade tip. In eq. (2), u_{out} was the outflow velocity on reference plane, the blade stagger angle was β , A_{ref} was the area of the reference plane and ω was the angular velocity of the rotor [8]:

$$M_m = - \int_{r_{hub}}^{r_{tip}} \rho \cdot u_{out}^2 \cdot (\tan \beta) \cdot r \cdot dA_{ref} + \int_{r_{hub}}^{r_{tip}} \rho \cdot u_{in} \cdot \omega \cdot r^2 \cdot dA_{ref} \quad (2)$$

which, after integration, yields

$$M_m = -\rho \cdot u_{out}^2 \cdot \tan \beta \cdot r \cdot A_{ref} + \rho \cdot u_{in} \cdot \omega \cdot r^2 \cdot A_{ref} \quad (2a)$$

The lift forces occurred due to velocity differences on rotors measured at the front and back surfaces. Equation (3) uses this relationship to compute the aerodynamic moment for number of rotor blades n , relative velocity $u_{in,rel}$ (with $u_{in} = u_{in,rel}$, for no preswirl), lift force coefficient C_L , drag force coefficient C_D , $\phi = \beta - \alpha$ (β = stagger angle of rotor blade, α = angle of attack of incoming flow).

$$M_a = \int_{r_{hub}}^{r_{tip}} \frac{1}{2} \cdot n \cdot \rho \cdot u_{in,rel}^2 \cdot L_{blade} \cdot (-C_L \cos \phi + C_D \sin \phi) \cdot r \cdot dr \quad (3)$$

resulting after integration in

$$M_a = \frac{1}{2} \cdot n \cdot \rho \cdot u_{in,rel}^2 \cdot L_{blade} \cdot (-C_L \cos \phi + C_D \sin \phi) \cdot \left(\frac{r_{tip}^2}{2} - \frac{r_{hub}^2}{2} \right) \quad (3a)$$

Averaging both moments results in

$$c_m = \frac{M_m + M_a}{\frac{\rho}{2} \cdot u_{in}^2 \cdot A \cdot L_{blade}} \quad (3b)$$

which, after substitution of the proper expressions gives c_m as:

$$c_m = \left(-\frac{2 \cdot r \cdot \tan \beta \cdot u_{out}^2 \cdot A_{ref}}{L_{blade} \cdot u_{in}^2 \cdot A} \right) + \left(\frac{2 \cdot \omega \cdot r^2 \cdot A_{ref}}{L_{blade} \cdot u_{in} \cdot A} \right) + \dots \\ \dots + \left(\frac{n \cdot u_{in,rel}^2}{A \cdot u_{in}^2} \right) (-C_L \cdot \cos \phi + C_D \cdot \sin \phi) \left(\frac{r_{tip}^2}{2} - \frac{r_{hub}^2}{2} \right) \quad (3c)$$

For a more realistic determination of the total moment, the bearing friction M_{reib} was added to the above moment as

a correction term. Equation (4a) shows the four most important types of friction. The main moments were rolling friction M_{rr} , dynamic friction M_{sl} , M_{seal} friction of seals and M_{drag} losses caused by flow of lubrication oil. These moments decreased the rotor speed. The bearing friction depended on, for example, the radial and axial forces, the kinematic viscosity, bearing diameters and other parameters [9]:

$$M_{reib} = M_{rr} + M_{sl} + M_{seal} + M_{drag} \quad (4a)$$

The rolling and dynamic friction forces considered as the most influential ones, the remaining were neglected. The correction term $c_{m,friction}$ becomes

$$c_{m,friction} = \frac{M_{rr} + M_{sl}}{\frac{\rho}{2} \cdot u_{in}^2 \cdot A \cdot L_{blade}} \quad (5)$$

The total relative moment coefficient was finally given by equation (5a)

$$c_{m,gesamt} = c_m - c_{m,reib} \quad (5a)$$

The rolling frictions was defined by equation (6)

$$M_{rr} = G_{rr} \cdot (\nu \cdot n_{speed})^{0,6} \quad (6)$$

with G_{rr} being the dimensionless rolling friction base value, ν the kinematic viscosity (mm^2/s) and n_{speed} the rotor speed (min^{-1}).

The dynamic friction was defined in equation (7)

$$M_{sl} = G_{sl} \cdot \mu_{sl} \quad (7)$$

with G_{sl} the dimensionless dynamic friction base value and μ_{sl} the coefficient of sliding friction.

The rolling friction was defined in equation (8)

$$G_{rr} = R_1 \cdot d_m^{1,96} \cdot \left(F_r + \frac{R_2}{\sin \alpha} \cdot F_a \right)^{0,54} \quad (8)$$

with R_1 and R_2 as dimensionless design coefficient, d_m - average radius of rotor (m), F_r - force in radial and F_a - force in axial direction (N) and $\sin \alpha$ defined in equation (9) as

$$\sin \alpha = 24,6 \cdot \left(\frac{F_a}{C_0} \right)^{0,24} \quad (9)$$

with C_0 as static load rating (kN).

The dimensionless dynamic friction base value was assumed to be defined in equation (10)

$$G_{sl} = S_1 \cdot d_m^{-0,145} \cdot \left(F_r^5 + \frac{S_2 \cdot d_m^{1,5}}{\sin \alpha} \right)^{\frac{1}{3}} \quad (10)$$

with S_1 and S_2 are dimensionless coefficients depending on bearing.

4. RESULTS

The aim of this work was the reproduction of an error curve for a typical turbine flow meter. A measured error curve for a meter with diameter DN80 (pressure 1 bar, medium air) is shown in Fig. 4, [10]. In this diagram, the deviation depending on flow rate is given. The behaviour of the meter was related to bearing friction forces, non-linear relation between inflow profile, viscosity, turbulence and flow rate. Optimally, an almost linear error curve should exist in a measurement range between 1:10 and 1:20. The typical strong increase of the negative deviation was due to the growing influence of friction. The slightly nonlinear profile at 70 % of Q_{max} is not understood yet.

In comparison, Fig.5 shows a simulated moment coefficient for turbine gas meter DN80 (diameter 0,074m), pressure 1bar air and maximum volume flow rate of $250\text{ m}^3\text{h}^{-1}$. The maximum rotor speed was 10.200 min^{-1} . The abscissa shows the volume flow rate in percent and the ordinate displays the dimensionless relative moment coefficient. The curves were normalized by the maximum flow rate, giving relative results.

In post-processing the planes of interests were flexibly defined. The inflow velocity at volume flow rate $250\text{ m}^3\text{h}^{-1}$ was $41,97\text{ ms}^{-1}$ and the outflow velocity was $32,51\text{ ms}^{-1}$. In Fig. 3 one can observe the result of flow speed visualization. For clarity, the rotor blades were not included. As mentioned above and expected, the velocity decreases throughout the cascade as a result of frictional losses. Local flow speed acceleration at the leading edges of rotor blades was clearly visible.

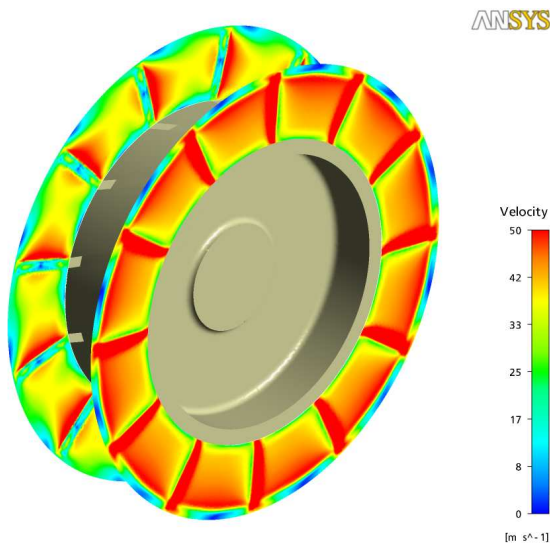


Fig. 3 Flow velocity visualization in the inflow and outflow planes at maximum volumetric flow of $250\text{ m}^3\text{h}^{-1}$

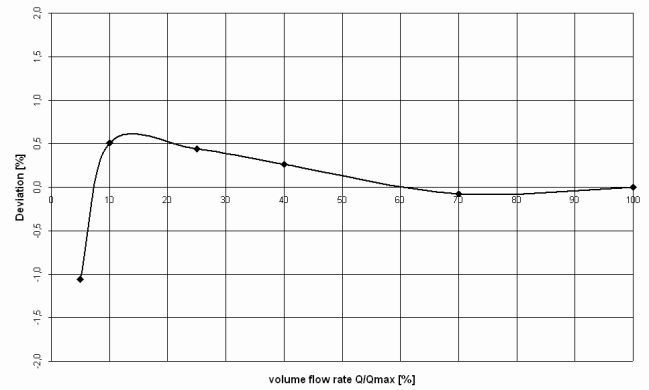


Fig. 4 Real error curve of turbine gas meter DN80 at 1 bar, air

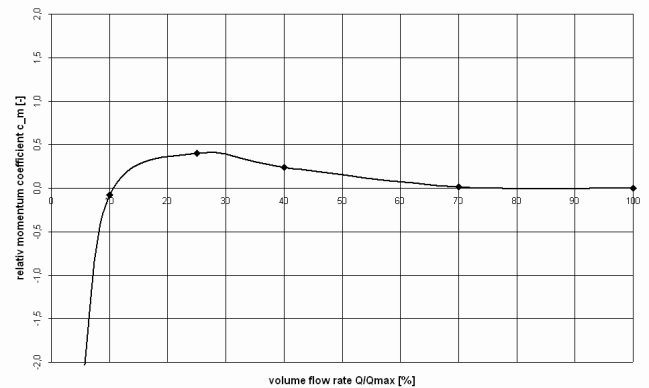


Fig. 5 Simulated moment coefficient curve of turbine gas meter DN80 at 1 bar, air

As testing procedure the rotor speed was adjusted in order to achieve an almost ideal error curve. At 10 % of Q_{max} the rotor speed had to be increased from 1020 min^{-1} to 1040 min^{-1} , at 25 % Q_{max} the rotor speed decrease was from 2550 min^{-1} to 2510 min^{-1} and at 40 % of Q_{max} the rotor speed had to decrease from 4070 min^{-1} to 4040 min^{-1} . Fig. 6 shows the adjusted curve (dotted line) in comparison to the original curve.

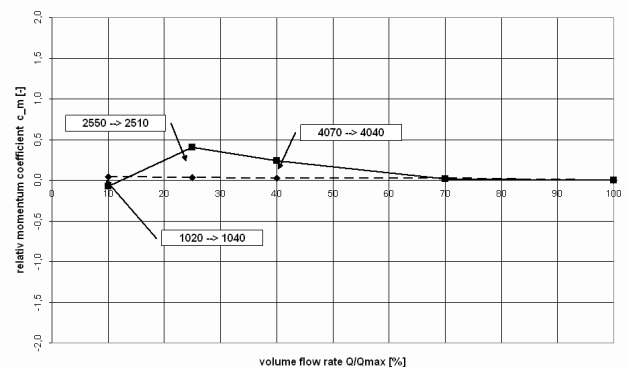


Fig. 6 Rotor speeds for as a function of flow rate

In reality, the meter should retain its correct behaviour even in presence of disturbed inflow profiles. [11]describes

a test procedure for mildly as well as severely disturbed inflows. This test standardized and generates the highest swirl and flow profile deformation. The mild disturbance was produced by a bend using a pipe of the same diameter as the meter. To simulate a control device as hardest pre-disturbance a two-elbow with semi cover plate will be used, please see Fig. 7.

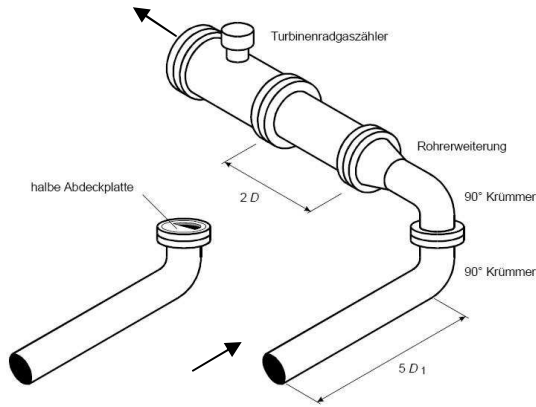


Fig. 7 Test configuration, OIML left-swirl high level disturbance [11]

The present CFD-simulation of the above configuration generated a double-vortex system with an almost radial flow. Near the pipe wall the fluid flowed parallel to the wall. The direction of rotation depended on the direction of the incoming flow into the given configuration. The direction of the swirl rotation depends directly on the direction of the incoming flow. The resulting flow field at the inflow was used subsequently in the present work in order to investigate the capability of the present method to account for upstream disturbances.

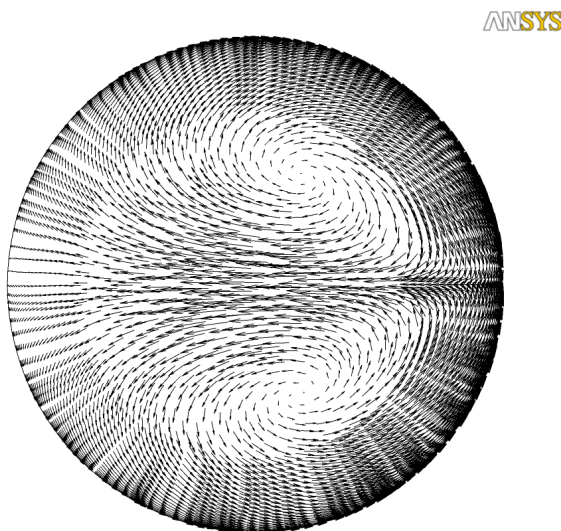


Fig. 8 Flow field visualized by vectors of velocity after severe incoming disturbance

Generally, in the case of swirl rotating in the opposite direction of the rotor, the rotor speed was reduced. The error curve consequently moved in negative direction because the

rotor was decelerated. This phenomenon was reproduced by the present method, as can be clearly seen in Fig. 9

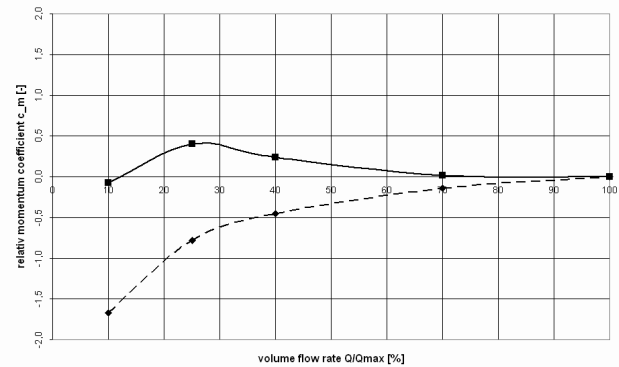


Fig. 9 Simulated curve under left-swirl high-level disturbance (dotted line)

The simulated error curve in Fig.5 displays a satisfactory correlation to the measured curve, except for a region at flow rates between 5% and 10%. The reason for this discrepancy could be that the assumption of the constant meter factor K in this area was inadequate and the mechanical friction was overestimated.

The practical meaning of the deviation of the rotor speed from the desired value at which the total moment is zero can be seen in Fig. 6. Here, the rotor speed has been modified (increased or decreased) in order to obtain zero torque. The amount of speed correction is shown in this picture for the corresponding flow rates. An ideal meter would dynamically adjust the rotor speed to enforce strictly linear behaviour, but this procedure would require rather complex mechanism with moving parts, which would be neither practical nor according to the law.

The simulated curve, Fig. 9, obtained for strong disturbances upstream of the meter shows the correct tendency, but the predicted deviation was overestimated. The reason could be insufficient grid resolution within the meter, as many computational cells were needed for the simulation of the flow upstream of the meter.

In general, the “Numerical Test Rig for Turbine Gas Meter” worked very well. For special problems such as disturbed inflow conditions, the results were quantitatively in good agreement with the corresponding experimental data. However, twenty-six input parameters were to be specified for one given simulation. They all influence the subsequent simulation and its results to some degree and should be chosen with care.

In Fig. 10 an example of a parameter study is shown. Here, three geometric parameters in the gas meter were varied. Their effect on the meter behaviour can be estimated by carefully regarding the quality of the resulting plot of the error curve.

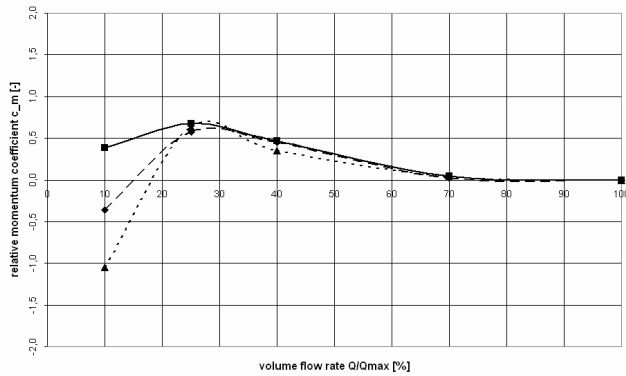


Fig. 10 Example of parameter studies

5. CONCLUSION

In general, the present results depended on several parameters being common to most CFD applications (turbulence model, positions planes of balances, mesh quality etc.). The present method of analyses of the flow field in general and the meter behaviour in particular was intended for practical use, especially for parameter variations during a design process.

The presented approach made engineering work faster and increased the level of knowledge in area of turbine gas meters. ANSYS CFX 11.0 and ICEM were used as readily available commercial software packages with considerable ease. In the future work, the method will be enhanced to be applicable for high-pressure operations and low flow rates.

5. REFERENCES

- [1] Hiegemann M., „Flow simulation of rotor in turbine gas meter“, original: „Berechnung der Strömung eines rotierenden Laufrades in einem Turbinenradgaszähler“, Ruhrgas AG, TAZN 4.5.20, 1998
- [2] Hilgenstock A., Hiegemann M., „Numerical simulation of operating behaviour of turbine gas meter“, original: „Numerische Simulation des Betriebsverhaltens eines Turbinenradgaszählers“, GWF 1999
- [3] Hüwener T., „Numerical investigation of transient flow in two-stage turbine gas meter“, original: „Numerische Untersuchung der instationären Strömung in einem zweistufigen Turbinenradgaszähler“, Dissertation, Universität Essen, 2001
- [4] von Lavante E., Banaszak U., Kettner T., Lötzt-Dauer V., "Numerical Simulation of Reynolds Number Effects in a Turbine Flow Meter"
- [5] von Lavante E., Lazaroski N., Maatje U., Kettner T., Lötzt-Dauer V., "Numerical Simulation of Unsteady Three - Dimensional Flow Fields in a Turbine Flow Meter "
- [6] von Lavante E., Banaszak U., Dietrich H., Lötzt-Dauer V., „Numerical simulation of flow field in turbine gas meter“, original: „Numerische Simulation des Strömungsfeldes eines Turbinenradgaszählers“, GWF 2006
- [7] Sun L., Zhou Z., Zhang T., "Numerical Simulation of Turbine Flow meters Three - Dimensional Flow Fields", Proceedings of the 6th World Congress in Intelligent Control and Automation, June 21 - 23, 2006, Dalian China
- [8] Stoltenkamp P.W., Dynamics of turbine flow meter, TU Eindhoven, Doctoral thesis, 2007
- [9] SKF - product catalogue, 2008
- [10] Data material of RMG Messtechnik GmbH
- [11] PTB – Physikalisch Technische Bundesanstalt, Technical Guideline G13 (Metering devices for Gas), Issue: 03/05, original: Technische Richtlinie G13 (Messgeräte für Gas), Ausgabe: 03/05